ISSN 2436-5173 (Online)

Metallomics Research

Vol.2/No.2
June 2022

Japan Society for
Biomedical Research on Trace Elements

Metallomics Research

Vol.2/No.2
June 2022
ISSN 2436-5173 (Online)

Japan Society for
Biomedical Research on Trace Elements

Index

Editorial Office

Seishinsha, co. Ltd.,
Japan society for Biomedical Research on Trace Elements
2-8-13 Fukashi, Matsumoto-shi, Nagano 390-0815, Japan
Tel: +81-263-32-2301
Fax: +81-263-36-4691
Editorial Office: brte-post@seisin.cc
URL: https://www.brte.org/
https://metallomicsresearch.brte.org/

Metallomics Research 2022 (2) #MR202202

Review https://metallomicsresearch.brte.org

Unraveling the new biological roles and possible applications of phytosiderophores in plants and mammals

Yoshiko Murata[1*], Jun Murata[1], Kosuke Namba[2]

[1]Bioorganic Research Institute, Suntory Foundation for Life Sciences, Kyoto 619-0284, Japan
[2]Department of Pharmaceutical Sciences, Tokushima University, Tokushima 770-8505, Japan

Abstract

Iron is an essential element for all living organisms. The ability of plants to absorb inorganic iron from soil is important not only for plants but also for mammals, which ultimately rely on plants as their nutrient source. In contrast to most plant species, Poaceae plants, including rice, have developed a distinct chelation strategy to efficiently acquire insoluble soil iron using iron-chelating substances such as mugineic acid (MAs), called phytosiderophores. Genes involved in the biosynthesis and transport of MAs and their resulting iron(III)-MA complexes across membranes have been identified. On the other hand, an efficient short-step synthesis of the substrates MA and 2′-deoxymugineic acid (DMA) has enabled a sufficient supply of these compounds. Furthermore, owing to the chemical synthesis of proline-2′-deoxymugineic acid (PDMA), a cost-effective analog of DMA, the effectiveness of phytosiderophores in promoting rice growth in alkaline soil has been demonstrated at an experimental field scale. Nicotianamine (NA), an MAs precursor essential for metal translocation within plant tissues, was recently shown to be absorbed as an iron(II) complex in the mouse small intestine by an amino acid transporter. The discovery of the biological role of NA in iron absorption by the small intestine not only highlights the biological significance of NA across the plant and animal kingdoms but also opens new possibilities for biofortification approaches. Here, we discuss the recent findings in MA research in terms of plant growth, application in agriculture, and the emerging nutraceutical value of NA in iron absorption in mammals.

Key words: phytosiderophore, iron uptake, mugineic acid, nicotianamine, transporter

Statements about COI: The authors declare no conflict of interest associated with this manuscript.

*Correspondence:
Yoshiko Murata Ph.D.
Bioorganic Research Institute, Suntory Foundation for Life Sciences
8-1-1 Seikadai, Seika-cho, Soraku-gun, Kyoto 619-0284, Japan
Tel: +81 774 66 1950, Fax: +81 774 98 6292
E-mail: murata@sunbor.or.jp

Received: March 31, 2022
Accepted: May 23, 2022
Released online: June 30, 2022

Abbreviations:

Dcytb; Duodenal cytochrome B, DMA; 2′-deoxymugineic acid, DMT1; divalent metal transporter1, HEPH; hephaestin, HvYS1; *Hordeum vulgare* yellow stripe1, IRT1; iron-regulated transporter1, FPN1; ferroportin, FRO; ferric-chelate reductase, MA(s); mugineic acids, NA; nicotianamine, PAT1; proton-conjugated amino acid transporter1, PDMA; proline-2′-deoxymucinic acid, YS1/YSL; yellow stripe1/yellow stripe1-like, ZmYS1; *Zea mays* yellow stripe1

Introduction

Iron is an essential mineral for redox reactions, electron transfer reactions, and enzymatic activity in living systems [1].

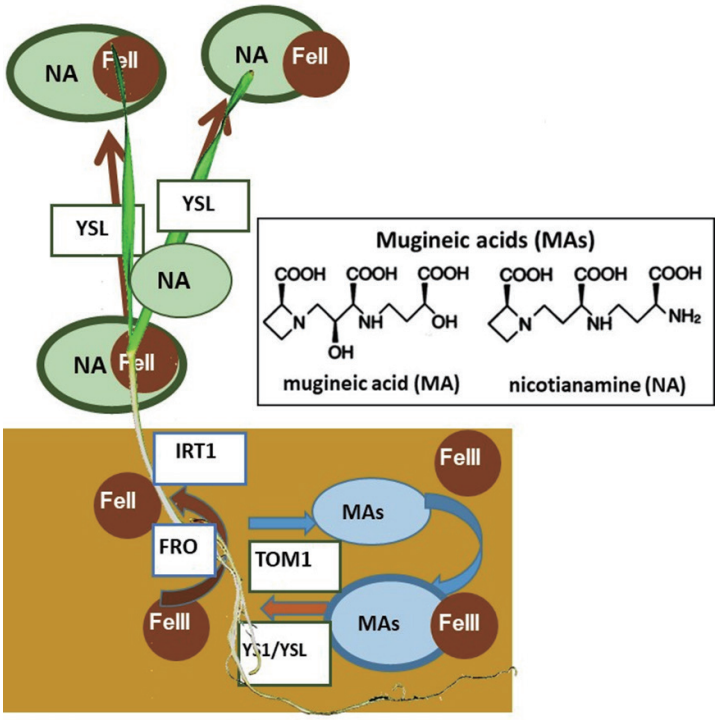

Figure 1. **Strategies by which plants absorb iron from soil**
Plants other than those belonging to Gramineae reduce Fe(III) to Fe(II) by reductase ferric-chelate reductase (FRO) and absorb iron through the Fe(II) transporter iron-regulated transporter1 (IRT1). On the other hand, gramineous plants secrete mugineic acids (MAs) into the soil via the TOM1 transporter, and iron intake occurs through the MAs-Fe(III) complex, mediated by the specific transporter yellow stripe 1/yellow stripe1-like (YS1/YSL). Nicotianamine (NA), present in all plants, plays a role in iron transport by forming the NA-Fe(II) complex.

Considering the food chain, living organisms ultimately obtain the nutrient iron from plants [2, 3]. Therefore, the ability of plants to absorb iron through their roots is of great importance to the entire living world. The proportion of iron present in the Earth's crust is approximately 5%, making it the fourth most abundant element after oxygen, silicon, and aluminum [4]; however, it is usually present in an oxidized, trivalent, water-insoluble form, which is not available for plants. Calculations show that for every unit increase in soil pH, the solubility of iron decreases by 1/1000 [5]. Therefore, approximately 30% of the world's neutral to alkaline soils are iron-deficient for plants, making them unsuitable for farming [6]. Plants have developed two major strategies for efficient iron absorption: reduction and chelation (**Figure 1**) [7]. Plants generally reduce iron(III) (ferric iron) to iron(II) (ferrous iron) by the enzyme ferric-chelate reductase (FRO) [8] and taking up iron(II) through the iron-regulated transporter1 (IRT1) present in the root epidermis [9]. By contrast, Poaceae plants synthesize and secrete phytosiderophores such as mugineic acids (MAs) through TOM1 transporter [10] in response to iron-deficiency [7]. The secreted MAs form water-soluble complexes with iron(III), which are then absorbed through the yellow stripe1/yellow stripe1-like (YS1/YSL) transmembrane transporter [11].

The structure of MA was first determined in 1978 by the Japanese group [12-14]. Takagi found that barley roots secreted iron-solubilizing substance from the roots in response to iron-deficiency [12]. Subsequently, Takemoto, Nomoto, and Takagi determined the structures of the substances and gave the name mugineic acids, which mean a kind of amino acid secreted from barley roots in Japanese [12, 13]. The biosynthetic pathway of MAs has been elucidated, in which L-methionine (Met) serves as a precursor for all known MAs [14-16], while Met is produced through the methionine cycle [15, 17]. All MAs share the same pathway from L-Met to 2′-deoxymugineic acid (DMA) via nicotianamine (NA), but the subsequent steps differ among plant species and cultivars. Most genes involved in phytosiderophore synthesis have been cloned, including those encoding adenine phosphoribosyl transferase (APRT), S-adenosylmethionine synthetase (SAMS), NA synthase (NAS), NA aminotransferase (NAAT), iron-deficiency-specific clones IDS2 and IDS3, and dioxygenases that hydroxylate the C-3 and C-2' positions of MA [4,17-22]. All these genes were specifically induced in plant roots under iron deficiency conditions. Two cis-acting elements of the barley iron-deficiency-specific clone 2 (*IDS2*) promoter, the iron-deficiency-responsive elements 1 and 2 (IDE1 and IDE2),

were involved in promoting iron-deficiency inducibility [23]. The secretion of phytosiderophores exhibits a distinct circadian rhythm [14]. The secretion time is likely controlled by the temperature around the roots [24]. The discovery of MAs by Japanese researchers has recently led to the elucidation of the mechanisms underlying iron absorption and iron transport in plants and mammals [25].

These studies establish that MAs are biologically important for grass plants and are biosynthesized at the expense of methionine through unique enzymatic reactions. However, since acquiring a large amount of naturally occurring MAs has been technically challenging, not much has been elucidated until recently as to whether the application of MAs to plants is sufficient for complementing the inhibited plant growth under iron-deficient conditions at the field experiment scale. Moreover, whether the phytosiderophores are utilized outside the plant kingdom has not been well understood. This review provides a brief overview of the effects of MAs on plant growth, possible agricultural impacts of the practical use of chemically synthesized MAs as 'natural' fertilizers, and the emerging nutraceutical value of NA in iron absorption in mammals.

YS1/YSL transport selectivity

Zea mays yellow stripe1 (ZmYS1) is a transporter of DMA-iron complexes that was first identified in 2001 using maize (*Zea mays*) mutant with yellow-white leaves (chlorosis) due to iron deficiency [26] ZmYS1 was reported to transport not only iron but also various metals complexed with DMA and the divalent NA-iron complex [27]. On the other hand, the absorption of metal complexed with MA in barley (*Hordeum vulgare*) was studied using various radio isotope-labeled metals. It was found that iron complexes were specifically absorbed [28]. Therefore, barley seemed to have a transporter with a substrate selectivity different from that of maize. We isolated and identified a 2430 bp (678 amino acid) long cDNA of the barley transporter *Hordeum vulgare* yellow stripe1 (*HvYS1*), which shares 72.7% similarity with ZmYS1 [29]. Focusing on the sixth extramembrane loop with low homology of the amino acid sequences of HvYS1 and ZmYS1, about 40 amino acid residues in this region were analyzed by AGADIR software and CD measurements. The results showed that HvYS1 has an α-helical structure, whereas ZmYS1 has a random structure. HvYS1 and ZmYS1 chimeras containing these 40 amino acid residues were expressed in Xenopus oocytes and their transport activity was measured. These studies indicated that the sixth extramembrane loop was responsible for the substrate specificity of HvYS1 [30].

In addition to HvYS1 and ZmYS1, further studies have identified 18 and 5 YSL genes in maize and barley, respectively. Moreover, YSL family genes with amino acid sequence homology of approximately 60% have been identified in various plant species, including 18 from rice (*Oryza sativa*), eight from *Arabidopsis thaliana*, six from grape (*Vitis vinifera*), three from the metal-accumulating plant *Thlaspi caerulescens*, two from *Physcomitrella patens*, and 18 from *Brachypodium distachyon* [11,31,32]. The substrates transported by these YSLs have been reported and are summarized in **Table 1** [26, 27, 29, 33-43]. The sequence similarity between these YSL transporters and HvYS1 within the 40 amino acid residues in the sixth extramembrane loop is relatively low. OsYSL15 [36, 37] and OsYSL18 [38], which transport the iron-MA complex in rice, as well as HvYS1, had the highest α-helix percentage of 17.1%. However, recent studies have demonstrated that all functionally characterized YSL transporters in *A. thaliana*, which do not biosynthesize MAs, exclusively transport NA-metal complexes instead of MA-metal complexes [39-41, 43]. In fact, this is characteristic of YSL transporters that transport NA-metal complexes in the above-ground parts of plants. One example is the OsYSL2, which is expressed in the above-ground part of rice and transports Fe(II) and Mn(II) complexed with NA but not with MA [35]. Elucidating the factors that determine the metal complex transport selectivity of this YSL transporter is expected to lead to the prediction and modification of substrate selectivity in the future.

Development of an efficient synthetic method for mugineic acid and 2'-deoxymugineic acid

The genes participating in the biosynthesis of MAs in rice have been identified [19, 21, 44], thus raising the possibility of engineering rice plants that can acquire iron more efficiently. Rice has a lower resistance to iron-deficiency stress because it secretes a small amount of MAs than barley. On the other hand, when rice is grown under flooded conditions, iron-deficiency may not be a problem due to soil reduction. Furthermore, under flooded conditions, secretion of MA is not an efficient way to acquire iron due to diffusion of MA in soil solution. In rice plants that are easily transformed, resistance to salty alkaline soil was acquired when MA synthesis was enhanced or a proof of concept experiment was conducted. We are interested in whether it is more effective in the state of upland rice. The amount of MA secretion follows the order: barley > wheat, rye ≫ corn ≫ sorghum

Table 1. | YS1/YSL transport activities in different crops

plant	YS1/YSL transporter	substrate complex		No or weak substrate activity	method	Reference No.
		PS or NA	metal	metal		
Zea mays (corn)	ZmYS1	DMA(PS)	Fe(III)-		yeast	26
	ZmYS1	DMA(PS)	Fe(III)-, Cu(II)-	Zn(II)-	yeast	33
		NA	Fe(III)-	Fe(III)-, Zn(II)-, Cu(II)-		
	ZmYS1	DMA (PS)	Fe(III)-, Fe(II)-, Zn(II)-, Cu(II)-, Ni(II)-, Mn(II)-, Cd(II)-		oocytes, yeast	27
		NA	Fe(III)-, Fe(II)-, Ni(II)-			
	ZmYS1	DMA (PS)	Fe(III)-, Zn(II)-, Cu(II)-, Ni(II)-, Mn(II)-, Co(II)-		oocytes, yeast	29
		NA	Fe(II)-			
Hordeum vulgare (barley)	HvYS1	MA(PS)	Fe(III)-	Fe(II)-, Zn(II)-, Cu(II)-, Ni(II)-, Mn(II)-, Co(II)-	oocytes, yeast	29
		DMA(PS)	Fe(III)-			
		NA		Fe(II)-		
	HvYSL2	DMA (PS)	Fe(III)-, Zn(II)-, Cu(II)-, Ni(II)-, Mn(II)-, Co(II)-		oocytes	34
		NA	Fe(II)-			
Oryza sativa (rice)	OsYSL2	DMA (PS)		Fe(III)-, Mn(II)-	oocytes	35
		NA	Fe(III)-, Mn(II)-	Fe(III)-, Zn(II)-, Cu(II)-		
	OsYSL15	DMA (PS)	Fe(III)-		oocytes, yeast	36
		NA		Fe(III)-, Fe(II)-, Mn(II)-		
	OsYSL15	DNA (PS)	Fe(III)-		yeast	37
		NA	Fe(II)-			
	OsYSL18	DMA (PS)	Fe(III)-	Zn(II)-	oocytes	38
		NA		Fe(II)-, Zn(II)-		
Arabidopsis Thaliana	AtYSL1	NA	Fe(II)-		mutants in Arabi.	39
	AtYSL2	MA(PS)		Fe(II)-, Fe(III)-, Cu(II)	yeast	40
		NA	Fe(II)-, Cu(II)-	Fe(III)-,		
	AtYSL2	NA		Fe(II)-, Fe(III)-, Ni(II)	yeast	41
	AtYSL3	NA	Fe(II)-		mutants in Arabi.	42
Thlaspi caerulescens (metal accumulatrion plant)	TcYSL3	NA	Fe(II)-, Ni(II)-		yeast	43

PS; phytosiderophore DMA; deoxymugineic acid
MA; mugineic acid NA; nicotianamine

≫ rice [45]. Transgenic rice carrying the barley genes involved in MAs synthase, secretion, and transport has been reported to be tolerant of iron deficiency in alkaline soil [25, 46-48]. Hence, if MA can be easily synthesized, it is expected to be a useful fertilizer. MAs are amino acid derivatives consisting of three reductively coupled units of azetidine carboxylic acid, aspartic acid, and malic acid. The efficient coupling of these units is the key to their synthesis. Although many MA and DMA synthesis methods were reported [49-58], multiple steps were required to desorb the protecting group of each amino acid unit in all these methods. Therefore, we improved the synthetic route based on the new concept of minimizing the use of amino acid protecting groups and minimizing the isolation and purification of each synthetic intermediate, establishing a continuous one-pot coupling method in which unprotected amino acids and aldehyde equivalents are added one after another [59]. This simplified synthetic method afforded DMA in yields up to 55% from *N*-Boc-L-allylglycine and enabled many synthetic MAs for mechanistic studies of phytosiderophores. So far, this method has been further improved for supply of low cost analog of DMA, PDMA, on a large scale (vide infra) [60]. In addition, a unified approach to natural phydosiderophores was recently reported by Stanetty *et al* [61].

Effects of DMA or proline analogs on rice growth

Synthetic MAs seem to have a beneficial effect in approving iron-deficiency stress in rice [62, 63]. The hydroponic cultures of rice (Oryza sativa) seedlings show almost complete restoration in shoot height and soil-plant analysis development (SPAD) values after treatment with 3–30 μM DMA at high pH (pH 8.0), compared with untreated control seedlings at normal pH (pH 5.8). Surprisingly, DMA application also increased nitrate reductase activity and the expression of genes encoding high-affinity nitrate transporters and nitrate reductases, all of which were otherwise considerably lower under high pH conditions. These data suggest that exogenous DMA not only plays a vital role in facilitating the uptake of environmental iron but also orchestrates iron and nitrate assimilation for optimal growth under high pH conditions. Since MAs showed better growth improvement than other synthetic iron chelators, such as EDTA, MAs may have potential for field application in alkaline soil [62, 63].

The efficient synthesis of DMA made it possible to conduct soil experiments with the addition of DMA. However, the instability of the four-membered ring of DMA and the extremely high cost of L-azetidine-2-carboxylic acid, the raw material for this four-membered ring, become a major limiting factor for the practical use of DMA as a fertilizer. Therefore, a recent study synthesized various analogs of L-azetidine-2-carboxylic acid substituted with stable and inexpensive amino acids and evaluated the intracellular transport activity of their trivalent iron chelates using insect cells expressing *HvYS1*. Results showed that PDMA, i.e., DMA modified with L-proline had an iron complex transport activity similar to DMA [60]. Because L-proline is a natural amino acid available at a low cost, the synthesis cost of PDMA was reduced to 1/1000–1/10000 in comparison to DMA, thus solving the raw material cost problem. Furthermore, while soil microorganisms degrade natural MAs in 1 day, PDMA takes approximately one month to be degraded, thus maintaining its effectiveness over a long time. Because PDMA is degradable, it can be used as an environmentally friendly fertilizer. Therefore, an improved synthetic method suitable for the quantitative synthesis of PDMA was developed based on the above synthesis of DMA [60], and a trial was conducted. The results showed that PDMA was approximately ten times more effective than the existing iron chelators in restoring iron deficiency in alkaline soil (**Figure 2**) [60].

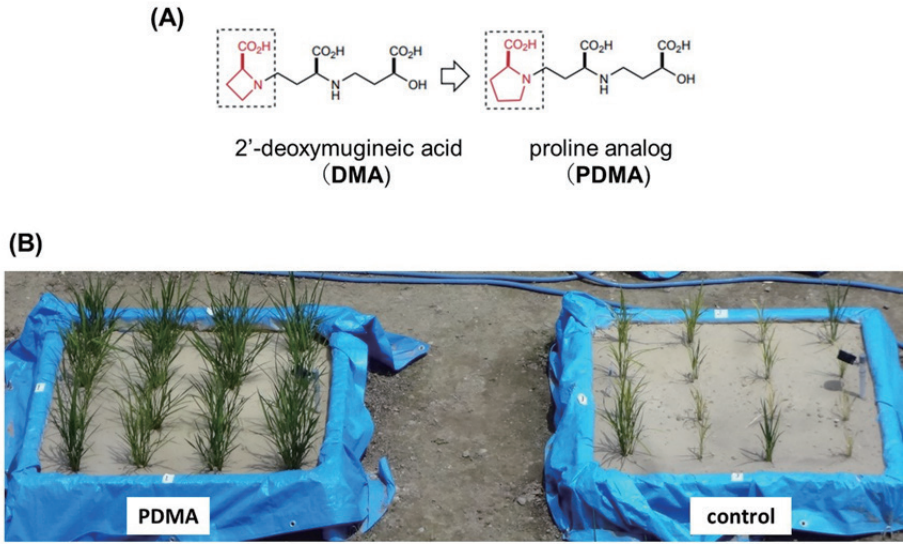

Figure 2. Effect of PDMA on rice plants grown in alkaline soil
(**A**) Structure of synthetic DMA analog PDMA.
(**B**) Four-week-old rice plants were treated with 30 μM PDMA (left) or without PDMA (right). (Provided by Dr. Motofumi Suzuki, Aichi Steel Corporation)

Iron uptake mediated by nicotianamine in the small intestine.

Iron deficiency, including severe anemia, occurs worldwide and therefore effective remedies are desired. People in Southeast Asia, including the Japanese, consume more than 85% of the iron in the form of non-heme iron from plant foods [64, 65]. Humans ultimately depend on crops for iron supply; therefore, iron availability to crops is essential [66]. Iron forms a complex with NA

that transports it mainly to plant stems, leaves, flowers, seeds and fruits. Activation of *OsNAS*, which encodes rice NA synthase [22], leads to an increase in iron concentration in the leaves and seeds of rice [67-69]. Recently, it was reported that hemoglobin levels increased in mice fed with transgenic rice overexpressing NA synthase [70]. The authors concluded that increasing the NA amount in transgenic rice also increased iron content, resulting in a higher iron in mice than in those fed with wild-type rice. On the other hand, soybean (*Glycine max*) grains and soy sauce contain a large amount of NA, which is an inhibitor of angiotensin-converting enzymes and then decreases blood pressure in hypertensive mice [71-73]. A recent study with quantitative analysis of NA in plasma showed that it was not decomposed after digestion but carried into the blood [72, 73]. Therefore, it seems that iron-chelating compounds produced by soybean, such as NA, are involved in iron absorption and transport in humans.

Iron absorption in humans mainly occurs in the duodenum; iron is absorbed as heme iron from animal foods and as inorganic iron from plant foods [74]. Since inorganic iron exists in a trivalent state, it is reduced to divalent iron by the reductase duodenal cytochrome B (Dcytb) [75] present in the small intestinal lumen. It is transported into the cell via the divalent metal transporter1 (DMT1) [76, 77]. The incorporated iron is stored as ferritin or transported via ferroportin1 (FPN1) on the basolateral cell membrane [78-80]. It is then oxidized by hephaestin (HEPH) to form iron(III), which binds to transferrin [81]. The mammalian absorption mechanism of inorganic iron or nonheme iron, which is abundant in plant foods uses the Dctyb/DMT1 pathway (reducion to divalent iron by Dcytb and transport into the cell via DMT1) in the duodenum [74] (**Figure 3**).

It has been reported that *Dcytb* is not essential in mice because knocking out this gene from small intestinal epithelial cells did not lead to iron deficiency [82]. Therefore, it is suggested that there is an iron absorption mechanism that is not explained yet and that NA, which is essential for iron transport in plants, is also involved in iron transport between cells in mammals. Since the NA-Fe(II) complex transporters YS1/YSL of plants belong to a family of oligopeptide transporters [83, 84], they possess trans oligopeptides and amino acids from the solute carrier (SLC) family involved in absorption in the small intestine [85, 86]. Through screening of transporters, a proton-conjugated amino acid transporter1 (PAT1; SLC36A1) was found in the small intestinal epithelial cells [87] and showed a transport activity similar to that of the NA-iron(II) complex (**Figure 3**) [88]. PAT1 was expressed in *Xenopus* oocytes for its electrophysiological activity measurement, revealing that NA-Fe(II) is transported

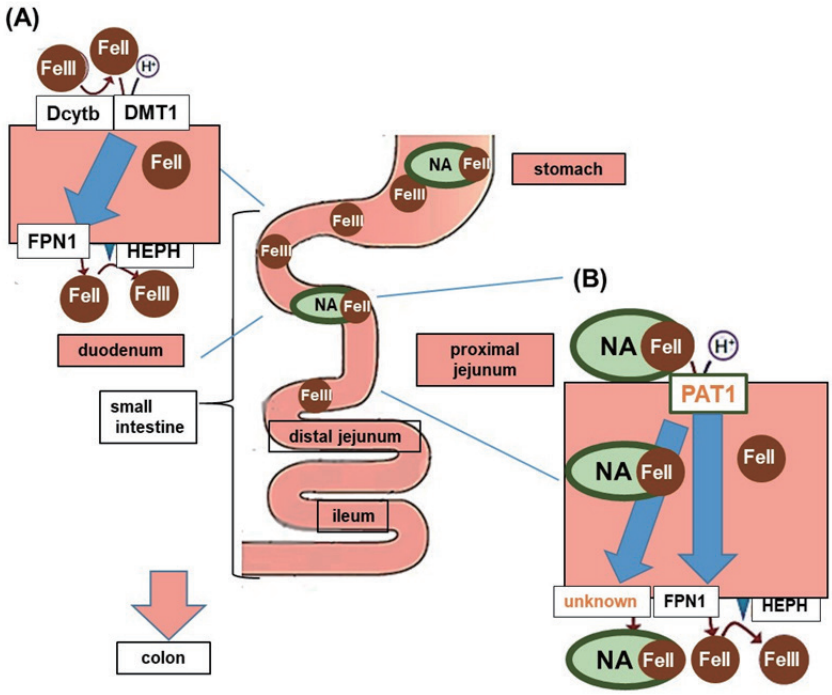

Figure 3. **Iron absorption mechanism in mammals**
In mammals, iron ingested from plant food is reduced to ferrous iron in the duodenum by duodenal cytochrome B (Dcytb) and is absorbed by the divalent metal transporter1 (DMT1).
(**A**) The incorporated iron is transported via ferroportin (FPN1) and oxidized by hephaestin (HEPH).
(**B**) It has been revealed that the nicotianamine (NA)-Fe(II) complex is absorbed by the amino acid transporter proton-conjugated amino acid transporter 1 (PAT1) in the proximal jejunum. It is undecided whether the incorporated NA-Fe(II) complex is transported as it is or as free iron by FPN1.

by PAT1. In addition, NA-^{59}Fe(II) oral administration in mice showed a high iron intake 30 min after administration in the proximal jejunum, where *PAT1* expression was also observed. In contrast, when free ^{59}Fe(II) was administered, iron absorption and *DMT1* expression were observed in the duodenum, indicating that free iron has an absorption site different from that of the NA-iron(II) complex (**Figure 3**) [88, 89]. Furthermore, when comparing NA-^{59}Fe(II) and ^{59}Fe(II) 5 h after administration to mice, NA-^{59}Fe(II) complex administration resulted in a higher absorption rate of ^{59}Fe in the spleen and kidney. The ferrous iron was given with a high dose of ascorbic acid; absorbed ferrous iron without NA can cause intravascular hemolysis and/or hemorrhagic gastric ulcer via Fenton reaction. Subsequently, hemoglobin level was decreased in mice given ferrous iron without NA. On the other hand, NA may have prevented the hemolysis, and the hemoglobin level was not changed or a little increased from the baseline. These results probably demonstrate the effect of NA on iron absorption in mice [88]. Further comparison of long-term administration experiments in mice of iron or NA-iron complex is required.

Conclusion

Here, we explained the absorption mechanism of mugineic acid in plants and its application, and the iron absorber in the small intestine by the precursor nicotianamine of mugineic acid in plant foods. Research on MAs and their analogs will contribute to solving the problem of food shortages caused by population growth and to the greening of poor soil on a global level. On one hand, MAs could be used to develop environmentally friendly fertilizers of iron. On the other hand, NA is useful for iron uptake and the efflux of excess iron in mammals. Free iron elicits a Fenton reaction, which sometimes causes ferroptosis [90] implicated in pathological cell death associated with degenerative diseases (*e.g.*, Alzheimer's, Huntington's, and Parkinson's diseases), carcinogenesis, stroke, intracerebral hemorrhage, traumatic brain injury, ischemia-reperfusion injury, and kidney degeneration [91]. Therefore, NA may be preferable for use in chelation therapy. The molecular mechanism that regulates iron absorption by nicotianamine remains unclear, and the regulatory mechanism of iron complex transporters in the small intestine needs to be elucidated. Further research revealing these points provides new insights for improving iron nutrition and contributes to human health. Generally, there are two main strategies for iron acquisition in biological organisms: reduction

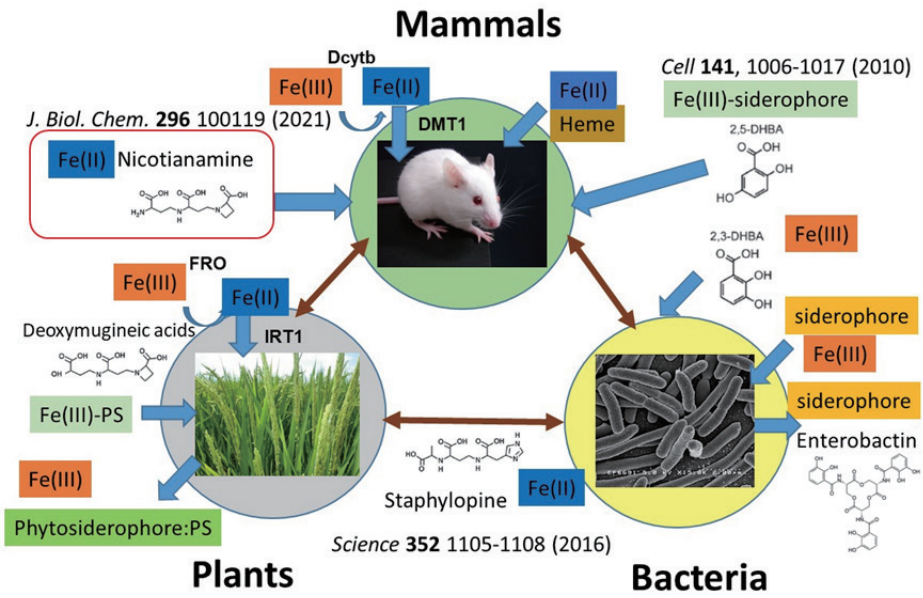

Figure 4. **Common molecules functioning in iron uptake in different biological systems**
There are two main strategies for iron acquisition in biological organisms: reduction and chelation. Plants have FRO/IRT1 and phytosiderophores systems. Bacteria are known to produce siderophores that form complexes with Fe(III) for example enterobactin. *Staphylococcus aureus* has been shown to biosynthesize staphyropine, which is an NA-like metallophore that forms a complex with Fe(II) recently. Mammals have iron uptake system in intestine; Deytb/DMT1 uptake Fe(III) and heme transport heme (Fe(II)) in duodenum and PAT1 transport NA-Fe(II) in the proximal jejunum. Recent studies have identified the mammalian siderophore as a low molecular weight 2,5-dihydroxybenzoic acid similar to the 2,3-dihydroxybenzoic acid found in the bacterial siderophore. Bacterial, plant and mammalian siderophores are becoming known to have similar iron absorption mechanisms.

and chelation. Bacteria are known to produce siderophores that form complexes with Fe(III). Recent studies have identified as mammalian siderophore a low-molecular-weight 2,5-dihydroxy benzoic acid with similarities to the 2,3-dihydroxy benzoic acid found in bacterial siderophores [92]. *Staphylococcus aureus* has been shown to biosynthesize staphyropine, which is an NA-like metallophore that forms a complex with Fe(II) [93, 94] (**Figure 4**). The structure of bacterial siderophores and respective transporters are versatile in general. However, the discovery of NA-like staphyropine from bacteria and the putative function of NA in the small intestine suggests the functional and structural convergence of NA as an iron chelator across three kingdoms.

Acknowledgments

We thank Dr. Hiroyuki Kimura and Dr. Hidekazu Kawashima from the Kyoto Pharmaceutical University for using mice and radioisotopes at the Radioisotope Research Center. This work was supported by JSPS (KAKENHI) Grant Numbers JP25350973 and JP16K01927.

References

[1] Kaplan J, Ward DM: The essential nature of iron usage and regulation. Curr Biol 23: 438-443, 2013.

[2] Briat JF, Curie C, Gaymard F: Iron utilization and metabolism in plants. Curr Opin Plant Biol 10: 276-282, 2007.

[3] Colangelo EP, Guerinot ML: Put the metal to the petal: metal uptake and transport throughout plants. Curr Opin Plant Biol 9: 322-330, 2006.

[4] Mori S: Iron acquisition by plants. Curr Opin Plant Biol 2: 250-253, 1999.

[5] Wallance A, Lunt OR: Iron chlorosis in horticultural plants, a review. Proc Am Soc Hort Sci 75: 819-841, 1960.

[6] Marschner H, Römheld V, Kissel M: Different strategies in higher plants in mobilization and uptake of iron. J Plant Nutr 9: 695-713, 1986.

[7] Römheld V, Marschner H: Evidence for a specific uptake system for iron phytosiderophores in roots of grasses. Plant Physiol 80: 175-180, 1986.

[8] Robinson NJ, Procter CM, Connolly EL, Guerinot ML: A ferric-chelate reductase for iron uptake from soils. Nature 397: 694-697,1999.

[9] Vert G, Grotz N, Dédaldéchamp F, Gaymard F, Guerinot ML, Briat JF, Curie C: IRT1, an Arabidopsis transporter essential for iron uptake from the soil and for plant growth. Plant Cell 14: 1223-1233, 2002.

[10] Nozoye T, Nagasaka S, Kobayashi T, Takahashi M, Sato Y, et al: Phytosiderophore efflux transporters are crucial for iron acquisition in graminaceous plants. J Biol Chem 286: 5446-554, 2011.

[11] Conte SS, Walker EL: Genetic and biochemical approaches for studying the yellow stripe-like transporter family in plants. Curr Top Membr 69: 295-322, 2012.

[12] Takagi S: Naturally occurring iron-chelating compounds in oat- and rice-root washings: I. Activity measurement and preliminary characterization. Soil Sci Plant Nutr 22: 423-433, 1976.

[13] Takemoto T, Nomoto K, Fushiya S, Ouchi R, Kusano G, Hikino H, et al: Structure of Mugineic Acid, a New Amino Acid Possessing an Iron-Chelating Activity from Roots Washings of Water-Cultured *Hordeum vulgare* L. Proc Jpn Acad 54: 469-473, 1978.

[14] Takagi S, Nomoto K, Takemoto T: Physiological aspect of mugineic acid, a possible phytosiderophore of graminaceous plants. J Plant Nut 7: 469-477, 1984.

[15] Ma JF, Nomoto K: Two related biosynthetic pathways of mugineic acids in gramineous plants. Plant Physiol 102: 373-378, 1993.

[16] Ma JF, Shinada T, Matsuda C, Nomoto K: Biosynthesis of phytosiderophores, mugineic acids, associated with methionine cycling. J Biol Chem 270: 16549-16554, 1995.

[17] Shojima S, Nishizawa NK, Fushiya S, Nozoe S, Irifune T, Mori S: Biosynthesis of Phytosiderophores : In Vitro Biosynthesis of 2′-Deoxymugineic Acid from l-Methionine and Nicotianamine. Plant Physiol 93: 1497-1503,1990.

[18] Mori S, Nishizawa NK: Methionine as a dominant precursor of phytosiderophores in gramineae plants. Plant Cell Physiol 28: 1081-1092, 1987.

[19] Inoue H, Higuchi K, Takahashi M, Nakanishi H, Mori S, Nishizawa NK. Three rice nicotianamine synthase genes, OsNAS1, OsNAS2, and OsNAS3 are expressed in cells involved in long-distance transport of iron and differentially regulated by iron. Plant J 36: 366-381, 2003.

[20] Takahashi M, Yamaguchi H, Nakanishi H, Shioiri T, Nishizawa NK, Mori S. Cloning two genes for nicotianamine aminotransferase, a critical enzyme in iron acquisition (Strategy II) in graminaceous plants. Plant Physiol 121:947-956, 1999.

[21] Inoue H, Takahashi M, Kobayashi T, Suzuki M, Nakanishi H, Mori S, et al: Identification and localisation of the rice nicotianamine aminotransferase gene OsNAAT1 expression suggests the site of phytosiderophore synthesis in rice. Plant Mol Biol 66:193-203, 2008.

[22] Higuchi K, Watanabe S, Takahashi M, Kawasaki S, Nakanishi H, Nishizawa NK, et al: Nicotianamine synthase gene expression differs in

barley and rice under Fe-deficient conditions. Plant J 25:159-167, 2001.

[23] Kobayashi T, Nakayama Y, Itai RN, Nakanishi H, Yoshihara T, Mori S, Nishizawa NK: Identification of novel cis-acting elements, IDE1 and IDE2, of the barley IDS2 gene promoter conferring iron-deficiency-inducible, root-specific expression in heterogeneous tobacco plants. Plant J 36: 780-793, 2003.

[24] Ma JF, Ueno H, Ueno D, Rombolà A, Iwashita T: Characterization of phytosiderophore secretion under Fe deficiency stress in Festuca rubra. Plant and Soil 256: 131-137, 2003.

[25] Kobayashi T, Nakanishi H, Nishizawa NK: Recent insights into iron homeostasis and their application in graminaceous crops. Proc Jpn Acad 86: 900-13, 2010.

[26] Curie C, Panaviene Z, Loulergue C, Dellaporta SL, Briat JF, Walker EL: Maize yellow stripe1 encodes a membrane protein directly involved in Fe(III) uptake. Nature 409: 346-349, 2001.

[27] Schaaf G, Ludewig U, Erenoglu BE, Mori S, Kitahara T, von Wirén N: ZmYS1 functions as a proton-coupled symporter for phytosiderophore- and nicotianamine-chelated metals. J Biol Chem 279: 9091-9096, 2004.

[28] Ma JF, Kusano G, Kimura S, Nomoto K: Specific recognition of mugineic acid–ferric complex by barley roots. Phytochemistry 34: 599-603, 1993.

[29] Murata Y, Ma JF, Yamaji N, Ueno D, Nomoto K, Iwashita T: A specific transporter for iron(III)-phytosiderophore in barley roots. Plant J 46: 563-572, 2006.

[30] Harada E, Sugase K, Namba K, Murata Y: The helical propensity of the extracellular loop is responsible for the substrate specificity of Fe(III)-phytosiderophore transporters. FEBS Letters 590: 1-11, 2016.

[31] Yordem BK, Conte SS, Ma JF, Yokosho K, Vasques KA, Gopalsamy SN, et al: Brachypodium distachyon as a new model system for understanding iron homeostasis in grasses: phylogenetic and expression analysis of Yellow Stripe-Like (YSL) transporters. Ann Bot 108: 821-833, 2011.

[32] Curie C, Cassin G, Couch D, Divol F, Higuchi K, Le JM, et al: Metal movement within the plant: contribution of nicotianamine and yellow stripe 1-like transporters. Ann Bot 103: 1-11, 2009.

[33] Roberts LA, Pierson AJ, Panaviene Z, Walker EL: Yellow stripe1: Expanded roles for the maize iron-phytosiderophore transporter. Plant Physiol 135: 112-120, 2004.

[34] Araki R, Kousaka K, Namba K, Murata Y, Murata J: 2′-Deoxymugineic acid promotes growth of rice (*Oryza sativa* L.) by orchestrating iron and nitrate uptake processes under high pH conditions. Plant J 81: 233-246, 2015.

[35] Koike S, Inoue H, Mizuno D, Takahashi M, Nakanishi H, Mori S, Nishizawa NK: OsYSL2 is a rice metal-nicotianamine transporter that is regulated by iron and expressed in the phloem. Plant J 39: 415-424, 2004.

[36] Inoue H, Kobayashi T, Nozoye T, Takahashi M, Kakei Y, Suzuki K, et al: Rice OsYSL15 is an iron-regulated iron(III)-deoxymugineic acid transporter expressed in the roots and is essential for iron uptake in early growth of the seedlings. J Biol Chem 284: 3470-3479, 2009.

[37] Lee S, Chiecko JC, Kim SA, Walker EL, Lee Y, Guerinot ML, An G: Disruption of OsYSL15 leads to iron inefficiency in rice plants. Plant Physiol 150: 786-800, 2009.

[38] Aoyama T, Kobayashi T, Takahashi M, Nagasaka S, Usuda K, Kakei Y, et al: OsYSL18 is a rice iron(III)-deoxymugineic acid transporter specifically expressed in reproductive organs and phloem of lamina joints. Plant Mol Biol 70: 681-692, 2009.

[39] Jean M, Schikora A, Mari S, Briat JF, Curie C: A loss-of-function mutation in AtYSL1 reveals its role in iron and nicotianamine seed loading. Plant J 44: 769-782, 2005.

[40] DiDonato RJJr, Roberts LA, Sanderson T, Eisley RB, Walker EL: Arabidopsis Yellow Stripe-Like2 (YSL2): a metal-regulated gene encoding a plasma membrane transporter of nicotianamine-metal complexes. Plant J 39: 403-414, 2004.

[41] Schaaf G, Schikora A, Häberle J, Vert G, Ludewig U, Briat JF, et al: A putative function for the arabidopsis Fe-phytosiderophore transporter homolog AtYSL2 in Fe and Zn homeostasis. Plant Cell Physiol 46: 762-774, 2005.

[42] Waters BM, Chu HH, DiDonato RJJr, Roberts LA, Eisley RB, Lahner B, et al: Mutations in Arabidopsis yellow stripe-like1 and yellow stripe-like3 reveal their roles in metal ion homeostasis and loading of metal ions in seeds. Plant Physiol 141: 1446-1458, 2006.

[43] Gendre D, Czernic P, Conéjéro G, Pianelli K, Briat JF, Lebrun M, et al: TcYSL3, a member of the YSL gene family from the hyper-accumulator Thlaspi caerulescens, encodes a nicotianamine-Ni/Fe transporter. Plant J 49: 1-15, 2007.

[44] Bashir K, Inoue H, Nagasaka S, Takahashi M, Nakanishi H, Mori S, et al: Cloning and characterization of deoxymugineic acid synthase genes from graminaceous plants. J Biol Chem 281: 32395-32402, 2006.

[45] Ma JF, Nomoto K: Effective regulation of iron acquisition in graminaceous plants. The role of mugineic acids as phytosiderophores. Physiol Plant 97: 609-617, 1996.

[46] Kobayashi T, Nakanishi H, Takahashi M, Mori S, Nishizawa NK: Generation and field trials of transgenic rice tolerant to iron deficiency. Rice 1: 144-153, 2008.

[47] Masuda H, Kobayashi T, Ishimaru Y, Takahashi M, Aung MS, Nakanishi H, et al: Iron-biofortification in rice by the introduction of three barley genes participated in mugineic acid biosynthesis with soybean ferritin gene. Front Plant Sci 4:132, 2013.

[48] Masuda H, Aung MS, Nishizawa NK: Iron biofortification of rice using different transgenic approaches. Rice (N Y) 6:40, 2013.

[49] Ohfune Y, Tomita M, Nomoto K: Total synthesis of 2′-deoxymugineic acid, the metal chelator excreted from wheat root. J Am Chem Soc 103:2409-2410, 1981.

[50] Fushiya S, Sato Y, Nakatsuyama S, Kanuma N, Nozoe S: Synthesis of avenic acid a and 2′-deoxymugineic acid, amino acids possessing an iron chelating activity. Chem Lett 10:909-912, 1981.

[51] Matsuura F, Hamada Y, Shioiri TN: Total synthesis of 2′-deoxymugineic acid and nicotianamine. Tetrahedron 50:9457-9470, 1994.

[52] Jung YH, Kim CM: A formal asymmetric synthesis of Mugineic acid: An efficient synthetic route through chiral oxazolidinone. Arch Pharm Res 22:624-628, 1999.

[53] Matsuura F, Hamada Y, Shioiri TN: Total synthesis of mugineic acid. Efficient use of the phenyl group as the carboxyl synthon. Tetrahedron 49:8211-8222, 1993.

[54] Matsuura F, Hamada Y, Shioiri TN: Efficient synthesis of mugineic acid, a typical phytosiderophore, utilizing the phenyl group as the carboxyl synthon. Tetrahedron Lett 33:7917-7920, 1992.

[55] Miyakoshi K, Oshita J, Kitahara T: Expeditious synthesis of nicotianamine and 2′-deoxymugineic acid. Tetrahedron 57:3355-3360, 2001.

[56] Klair SS, Mohan HR, Kitahara T: A novel synthetic approach towards phytosiderophores: expeditious synthesis of nicotianamine and 2′-deoxymugineic Acid. Tetrahedron Lett 39:89-92, 1998.

[57] Singh SG: A short practical synthesis of 2′-deoxymugineic acid. Tetrahedron Lett 46:1419-1421, 2005.

[58] Shioiri TN: A new efficient synthesis of nicotianamine and 2 -deoxymugineic acid. Heterocycles 44:519-530, 1997.

[59] Namba K, Murata Y, Horikawa M, Iwashita T, Kusumoto S: A practical synthesis of the phytosiderophore 2′-deoxymugineic acid: A key to the mechanistic study of iron acquisition by graminaceous plants. Angew Chem Int Ed Engl 46: 7060-7063, 2007.

[60] Suzuki M, Urabe A, Sasaki S, Tsugawa R, Nishio S, Mukaiyama H, Yoshiko Murata, et al: Development of a mugineic acid family phytosiderophore analog as an iron fertilizer. Nat Commun 12: 1558, 2021.

[61] Kratena N, Gökler T, Maltrovsky L, Oburger E, Stanetty C: A unified approach to phytosiderophore natural products. Chem Eur J 27:577-580, 2021.

[62] Araki R, Kousaka K, Namba K, Murata Y, Murata J: 2′-Deoxymugineic acid promotes growth of rice (Oryza sativa L.) by orchestrating iron and nitrate uptake processes under high pH conditions. Plant J 81:233-246, 2015.

[63] Araki R, Namba K, Murata Y, Murata J: Phytosiderophores revisited: 2′-deoxymugineic acid-mediated iron uptake triggers nitrogen assimilation in rice (*Oryza sativa* L.) seedlings. Plant Sign. Behav.10: e1031940, 2015.

[64] Lopez A, Cacoub P, Macdougall IC, Peyrin-Biroulet L: Iron deficiency anaemia. Lancet 387: 907-916, 2016.

[65] World Health Organization (WHO) The Global Prevalence of Anaemia in 2011. Geneva, Switzerland 2015.

[66] Welch RM: The impact of mineral nutrients in food crops on global human health. Plant Soil 247: 83-90, 2002.

[67] Zheng L, Cheng Z, Ai C, Jiang X, Bei X, Zheng Y, et al: Nicotianamine, a novel enhancer of rice iron bioavailability to humans. PLoS One 5: e10190, 2010.

[68] Lee S, Jeon US, Lee SJ, Kim YK, Persson DP, Husted S, et al: Iron fortification of rice seeds through activation of the nicotianamine synthase gene. Proc Natl Acad Sci U S A 106: 22014-22019, 2009.

[69] Nozoye T, Kim S, Kakei Y, Takahashi M, Nakanishi H, Nishizawa NK: Enhanced levels of nicotianamine promote iron accumulation and tolerance to calcareous soil in soybean. Biosci Biotechnol Biochem 78: 1677-1684, 2014.

[70] Lee S, Kim YS, Jeon US, Kim YK, Schjoerring JK, An G: Activation of Rice nicotianamine synthase 2 (OsNAS2) enhances iron availability for biofortification. Mol Cells 33: 269-275, 2012.

[71] Kinoshita E, Yamakoshi J, Kikuchi M: Purification and identification of an angiotensin I-converting enzyme inhibitor from soy sauce. Biosci Biotechnol Biochem 57: 1107-1110, 1993.

[72] Hayashi A, Nakayama T, Murakami K, Aoyagi Y, Kimoto K: Effects of nicotianamine on blood pressure in Tsukuba hypertensive mice (THM). J Jpn Soc Nutr Food Sci 58: 315-321, 2005.

[73] Hayashi A, Kimoto K: Nicotianamine preferentially inhibits Angiotensin I-converting enzyme. J Nutl Sci Vitaminol 53: 331-336, 2007.

[74] Fuqua BK, Vulpe CD, Anderson GJ: Intestinal iron absorption. J Trace Elem Med Biol 26: 115-119, 2012.

[75] McKie AT, Barrow D, Latunde-Dada GO, Rolfs A, Sager G, Mudaly E, et al: An iron-regulated ferric reductase associated with the absorption of dietary iron. Science 291: 1755-1759, 2001.

[76] Gunshin H, Mackenzie B, Berger UV, Gunshin Y, Romero MF, Boron WF, et al: Cloning and characterization of a mammalian proton-coupled metal-ion transporter. Nature 388: 482-488, 1997.

[77] Hubert N, Hentze MW: Previously uncharacterized isoforms of divalent metal transporter (DMT)-1: implications for regulation and cellular function. Proc Natl Acad Sci U S A 99: 12345-12350, 2002.

[78] Kaplan J, Kushner JP: Mining the genome for iron. Nature 403: 711-713, 2000.

[79] McKie AT, Marciani P, Rolfs A, Brennan K, Wehr K, Barrow D, et al: A novel duodenal iron-regulated transporter, IREG1, implicated in the basolateral transfer of iron to the circulation. Mol Cells 5: 299-309, 2000.

[80] Abboud S, Haile DJ: A novel mammalian iron-regulated protein involved in intracellular iron metabolism. J Biol Chem 275: 19906-19912, 2000.

[81] Anderson GJ, Frazer DM: Current understanding of iron homeostasis. Am J Clin Nutr 106: 1559S-1566S, 2017.

[82] Gunshin H, Starr CN, Direnzo C, Fleming MD, Jin J, Greer EL, et al: Cybrd1 (duodenal cytochrome b) is not necessary for dietary iron absorption in mice. Blood 106: 2879-2883, 2005.

[83] Yen MR, Tseng YH, Saier MHJ: Maize Yellow Stripe1, an iron-phytosiderophore uptake transporter, is a member of the oligopeptide transporter (OPT) family. Microbiology 147: 2881-2883, 2001.

[84] Lubkowitz M: The OPT family functions in long-distance peptide and metal transport in plants. Genet Eng 27: 35-55, 2006.

[85] Hediger MA, Romero MF, Peng JB, Rolfs A, Takanaga H, Bruford EA: The ABCs of solute carriers: physiological, pathological and therapeutic implications of human membrane transport proteinsIntroduction. Pflugers Arch 447: 465-468, 2004.

[86] Perland E, Fredriksson R: Classification Systems of Secondary Active Transporters. Trends Pharmacol Sci 38: 305-315, 2017.

[87] Chen Z, Fei YJ, Anderson CMH, Wake KA, Miyauchi S, Huang W, et al: Structure, function and immunolocalization of a proton-coupled amino acid transporter (hPAT1) in the human intestinal cell line Caco-2. J Physiol 546: 349-361, 2003.

[88] Murata Y, Yoshida M, Sakamoto N, Morimoto S, Watanabe T, Namba K: Iron uptake mediated by the plant-derived chelator nicotianamine in the small intestine. J Biol Chem 296: 100195, 2021.

[89] Collins JF: Iron chelates hitch a ride on PAT1. J Biol Chem 296, 100418 2021.

[90] Dixon SJ, Lemberg KM, Lamprecht MR, Skouta R, Zaitsev EM, Gleason CE, et al: Ferroptosis: an iron-dependent form of nonapoptotic cell death. Cell 149: 1060-1072, 2012.

[91] Stockwell BR, Friedmann Angeli JP, Bayir H, Bush AI, Conrad M, Dixon SJ, et al: Ferroptosis: A regulated cell death nexus linking metabolism, redox biology, and disease. Cell 171: 273-285, 2017.

[92] Ghssein G, Brutesco C, Ouerdane L, Fojcik C, Izaute A, Wang S, et al: Biosynthesis of a broad-spectrum nicotianamine-like metallophore in Staphylococcus aureus. Science 352:1105-9 2016.

[93] Dertz EA, Xu J, Stintzi A, Raymond KN: Bacillibactin-mediated iron transport in Bacillus subtilis. J Am Chem Soc 128:22-23, 2006.

[94] Laffont C, Arnoux P: The ancient roots of nicotianamine: diversity, role, regulation and evolution of nicotianamine-like metallophores. Metallomics 12: 1480-1493, 2020.

Metallomics Research 2022 (2) #MR202204

Regular article https://metallomicsresearch.brte.org

Changes in the Renal Copper Concentration in Rats as a Function of Phosphorus Intake

Munehiro Yoshida*, Suzuno Ikeda, Ryota Hosomi, Kenji Fukunaga

Laboratory of Food and Nutritional Sciences, Faculty of Chemistry, Materials and Bioengineering, Kansai University

Summary

We have found that the renal copper concentrations are markedly decreased in rats fed a low-phosphorus diet or administered phosphate binders. To clarify the relationship between phosphorus intake and renal copper concentration, we examined the renal copper concentrations in rats fed three types of diet with different phosphorus content. Eighteen 4-week-old male Wistar rats were divided into 3 groups and fed either a low phosphorus diet (phosphorus concentration, 0.15%), a control diet (phosphorus concentration, 0.3%), or a high phosphorus diet (phosphorus concentration, 0.6%) for 4 weeks. The serum phosphorus concentration reflected the phosphorus intake, with the highest values in the high phosphorus diet group, control group, and low phosphorus diet group, in that order. In the liver, the low phosphorus diet group had a significantly lower copper concentration than the other two groups, but the difference was not large. The kidney copper concentrations were remarkably different among the groups, with the highest values in the high phosphorus diet group, control group, and low phosphorus diet group, in that order. There were no differences in the iron, zinc, and manganese concentrations among the groups, except for a higher liver iron concentration in the low phosphorus diet group. These results indicate that the renal copper concentration increases or decreases specifically in response to changes in the phosphorus intake.

Key words: renal coper, phosphorus intake, interaction between minerals

Statements about COI: The authors have no conflicts of interest directly relevant to the content of this article.

*Correspondence:
3-3-35 Yamate, Suita, Osaka 564-8680, Japan
Tel: +81 6 6368 0970 (cell phone number: +81 90 9990 1853)
E-mail: hanmyou4@kansai-u.ac.jp

Received: May 24, 2022
Accepted: August 01, 2022
Released online: August 18, 2022

Introduction

Phosphorus is an essential element in the formation of bone salts and cell membranes. It is also a material found in several nucleotides and high-energy phosphate compounds and is a major intracellular electrolyte. Thus, its excess or deficiency induces various health disorders [1]. However, the risk of specific dietary phosphorus deficiency is low because much of the phosphorus in the diet is protein bound [2]. In contrast, the high use of phosphate compounds in food additives may lead to excessive phosphorus intake [3].

Inadequate urinary excretion of phosphorus, such as in chronic renal failure, may increase the serum phosphorus level and cause ectopic calcification due to the binding of phosphate

with calcium [4]. If this calcification occurs in the coronary or cerebral arteries, it can induce fatal ischemic disease. For this reason, patients with chronic renal failure should take phosphate binders to inhibit the absorption of phosphorus in the diet and prevent hyperphosphatemia [5].

Because phosphorus is bound to dietary proteins, it is difficult to prepare a severely low phosphorus diet. But a phosphate binder can be administered to experimental animals to induce a low phosphorus state [6]. We found that the administration of phosphate binders, such as lanthanum carbonate or iron citrate, to normal rats decreased the copper concentration in the kidney [7,8]. This decrease in the renal copper concentration was also observed in rats fed a mildly low phosphorus diet [9], suggesting that the low phosphorus state caused the decrease, not the effect of the metals used in the phosphate binders.

No studies have been found to explain the phenomenon of a low phosphorus state reducing the kidney copper levels. Nor has the interaction between phosphorus and copper been examined in the first place. In the present study, to clarify the relationship between phosphorus intake and renal copper concentration, the effect of high phosphorus feeding on the renal copper concentration was examined.

Materials and methods

Animal feeding

The experimental protocol followed the Guide for the Care and Use of Experimental Animals issued by the Prime Minister's Office of Japan and was reviewed and approved by the Animal Ethics Committee of Kansai University (Approval No. 2005).

Eighteen 4-week-old male Wistar rats (SHIMIZU Laboratory Supplies Co., Kyoto) were divided into 3 groups. One group (control group) was fed a basal AIN93G diet (control diet) with a phosphorus concentration of 0.3% [10], and the other two groups (low phosphorus group and high phosphorus group) were fed a low phosphorus diet with a phosphorus concentration of 0.15% and a high phosphorus diet with a phosphorus concentration of 0.6%, respectively. The composition of each diet is summarized in **Table 1**. The low phosphorus diet was prepared by replacing potassium dihydrogen phosphate in the AIN93G

Table 1. | Composition of the experimental diet

	Low P diet	Control diet	High P diet
Ingredients (g/kg)			
Casein	200	200	200
Sucrose	100	100	100
Soybean oil	70	70	70
Corn starch	391.84	391.84	385.88
Gelatinized corn starch	132	132	132
Phosphorus-free mineral mixture[1)]	35	–	–
AIN93G mineral mixture	–	35	35
AIN93G vitamin mixture	10	10	10
Cellulose	50	50	50
Choline bitartrate	2.5	2.5	2.5
L-Cystine	3	3	3
NaH_2PO_4	–	–	11.62
NaCl[2)]	5.66	5.66	–
Phosphorus content (%)[3)]	0.15	0.30	0.60
Chloride ion (Cl^-) content (%)	0.68	0.50	0.16

[1)] Prepared by removing KH_2PO_4 from the AIN93G mineral mix and adding KCl to equalize the potassium concentration.
[2)] Added to equalize the sodium concentration.
[3)] Contains phosphorus derived from casein.

mineral mixture with potassium chloride, and the high phosphorus diet was prepared by adding sodium dihydrogen phosphate to the AIN93G diet. Sodium chloride was also added to the low phosphorus and control diets to equalize the sodium intake of each group. As a result, the chloride ion concentrations in the diets were highest in the low phosphorus diet, the control diet, and the high phosphorus diet, in that order.

During the feeding period, the animals ingested the diets and water (tap water) *ad libitum*. After feeding for 4 weeks, the livers, kidneys, and blood were collected under isoflurane (Fujifilm Wako Pure Chemical Co., Tokyo) anesthesia. Some of the blood was centrifuged at 1,500 x g for 15 minutes to obtain serum. The livers and kidneys were frozen in liquid nitrogen and stored at −30°C until analysis.

Analysis

One kidney and approximately 1 g of liver were heated with 5 mL nitric acid until there were no solids. The obtained solution was diluted with pure water and filtrated through a 0.45 μm filter, and zinc, iron, copper, and manganese were determined using an atomic absorption spectrophotometer (AA-7000, Shimadzu, Kyoto) or inductively coupled plasma mass spectrometer (ICPMS-2030, Shimadzu, Kyoto). In the analysis with ICPMS, ^{45}scandium was used as an internal standard. The other kidney was homogenized in 10 times volume of saline and centrifuged (105,000 x g, 60 minutes) to separate the soluble fraction and precipitate, and the respective copper concentrations were determined. Serum zinc and copper were measured using a commercial kit (Metalloassay LS, Metallogenics Co., Chiba).

Whole blood hemoglobin and serum total protein, triacylglycerol, total cholesterol, urea nitrogen, uric acid, chloride ion, calcium, magnesium, inorganic phosphorus, iron and total iron binding capacity were determined by Japan Medical Laboratory Co. (Kaizuka).

For each measurement, the differences among the groups were tested by one-way ANOVA followed by the Tukey's multiple comparison test. GraphPad Prism 7.0 (GraphPad Software, Inc., San Diego) was used as the statistical analysis application.

Results

The body weights and organ weights at the end of the feeding period, as well as water consumption and feed efficiency during the feeding period are summarized in **Table 2**. In the low phosphorus group, body weight and feed efficiency were lower than in the other two groups. However, this group had a higher kidney weight per body weight and drank more water during the feeding period. Although the exact amounts were not measured, the low phosphorus group also had a higher urine output. On the other hand, the high phosphorus group did not differ from the control group in terms of the body and organ weights.

The serum biochemical parameters and hemoglobin concentrations are shown in **Table 3**. The serum inorganic phosphorus concentrations reflected the dietary phosphorus concentrations and were highest in the high phosphorus group, control group, and low phosphorus group, in that order. No differences were observed between the high phosphorus group and the control group for the other parameters. On the other hand, the low phosphorus group had lower triacylglycerols and higher uric acid, calcium, and hemoglobin values than the other two groups. Serum copper also tended to be lower in the low phosphorus group, but the difference was not significant.

The iron, zinc, copper, and manganese concentrations in the liver and kidneys are shown in **Table 4**. In the liver, a significant accumulation of iron was observed in the low phosphorus group. The copper concentrations tended to be higher with a higher phosphorus intake, with significant differences between the high and low phosphorus groups. In the kidneys, on the other hand, there were notable differences in the copper concentrations among the groups. That is, the low phosphorus group had the lowest kidney copper concentration, while the high phosphorus group had significantly higher values than the control group. In other words, the kidney copper concentrations were lower when the phosphorus intake was low and higher when the phosphorus intake was high.

The kidneys were divided into soluble and insoluble fractions, and their respective copper concentrations were measured. As shown in **Figure 1**, in both fractions, the copper concentrations were significantly higher with increasing phosphorus intake.

Table 2. | Body weight, liver and kidney weights, and feed efficiency

	Low P	Control	High P	ANOVA
Body weight (g)	245.0 ± 8.1[a]	291 1 ± 3.1[b]	295.8 ± 4.0[b]	p<0.001
Feed efficiency[1)]	0.411 ± 0.018[a]	0.507 ± 0.009[b]	0.473 ± 0.008[b]	p<0.001
Water intake (mL/d)	41.7 ± 2.6[b]	36.3 ± 2.5[ab]	31.6 ± 2.7[a]	p=0.047
Liver weight (g/100 g body weight)	4.09 ± 0.14	4.05 ± 0.06	4.21 ± 0.10	NS[2)]
Kidney weight (g/100 g body weight)	0.82 ± 0.02[b]	0.74 ± 0.01[a]	0.71 ± 0.01[a]	p<0.001

Values are means ± SEM (n=6). Tukey's multiple comparison was performed when ANOVA was significant (p<0.05); means in the same row not sharing a common superscript differ significantly (p<0.05) in the multiple comparison.
[1)] Calculated from the formula: (body weight gain during the feeding period (g)) / (total food intake (g)).
[2)] NS: not significant

Table 3. | Serum biochemical parameters and hemoglobin concentration

	Low P	Control	High P	ANOVA
Serum biochemical parameters				
Total protein (mg/dL)	5.3 ± 0.1	5.3 ± 0.1	5.4 ± 0.1	NS[1)]
Triacylglycerol (mg/dL)	52 ± 5[a]	88 ± 16[b]	73 ± 15[b]	p=0.002
Total cholesterol (mg/dL)	76 ± 4	75 ± 5	79 ± 4	NS
Urea nitrogen (mg/dL)	21 ± 2	19 ± 1	18 ± 1	NS
Uric acid (mg/dL)	1.23 ± 0.06[b]	0.78 ± 0.09[a]	0.77 ± 0.05[a]	p<0.001
Chloride ion (mEq/L)	100 ± 1	101 ± 1	100 ± 1	NS
Calcium (mg/dL)	12.55 ± 0.21[b]	10.65 ± 0.14[a]	10.85 ± 0.06[a]	p<0.001
Magnesium (mg/dL)	1.82 ± 0.05	1.87 ± 0.03	1.85 ± 0.06	NS
Inorganic phosphorus (mg/dL)	4.53 ± 0.37[a]	7.02 ± 0.30[b]	8.13 ± 0.20[c]	p<0.001
Iron (μg/dL)	289 ± 18	288 ± 16	269 ± 23	NS
Transferrin saturation (%)	62.4 ± 5.2	58.2 ± 3.4	50.7 ± 4.3	NS
Zinc (μg/dL)	237 ± 11	231 ± 13	226 ± 19	NS
Copper (μg/dL)	119 ± 9	155 ± 18	152 ± 27	NS
Hemoglobin (g/dL)	14.0 ± 0.2[b]	13.5 ± 0.1[a]	13.5 ± 0.1[a]	p=0.007
Hematocrit value (%)	40.8 ± 0.6	39.9 ± 0.3	39.5 ± 0.3	NS

Values are means ± SEM (n=6). Tukey's multiple comparison was performed when ANOVA was significant (p<0.05); means in the same row not sharing a common superscript differ significantly (p<0.05) in the multiple comparison.
[1)] NS: not significant

Table 4. | Iron, zinc, copper, and manganese concentrations (μg/g) in liver and kidney

	Low P	Control	High P	ANOVA
Liver				
Iron	98.8 ± 5.5[b]	81.5 ± 3.1[a]	83.4 ± 3.6[ab]	p=0.020
Zinc	27.0 ± 0.5	26.9 ± 0.6	27.2 ± 0.9	NS[1)]
Copper	3.29 ± 0.05[a]	3.44 ± 0.05[ab]	3.53 ± 0.07[b]	p=0.030
Manganese	2.79 ± 0.08	2.94 ± 0.31	2.44 ± 0.15	NS
Kidney				
Iron	45.9 ± 1.6	46.9 ± 1.2	47.9 ± 0.6	NS
Zinc	19.7 ± 1.3	21.4 ± 1.1	21.3 ± 0.7	NS
Copper	4.26 ± 0.13[a]	12.19 ± 0.45[b]	17.75 ± 1.21[c]	p<0.001
Manganese	1.07 ± 0.05	1.18 ± 0.09	0.99 ± 0.03	NS

Values are means ± SEM (n=6). Tukey's multiple comparison was performed when ANOVA was significant (p<0.05); means in the same row not sharing a common superscript differ significantly (p<0.05) in the multiple comparison.

[1)] NS: not significant

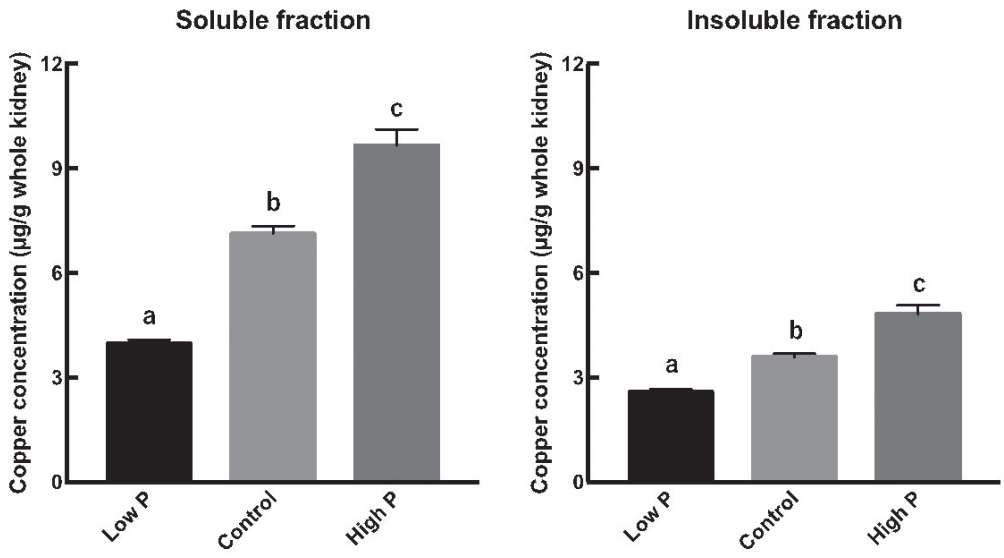

Figure 1. | Copper concentrations in soluble and insoluble fractions of the kidney
The height of the box and the length of the vertical line show the mean and SEM (n=6), respectively. Means in the same frame not sharing a common superscript differ significantly (p<0.05) in the Tukey's multiple comparison.

Discussion

In the present experiment, potassium dihydrogen phosphate was replaced with potassium chloride in the mineral mixture for the preparation of the low phosphorus diet. Because sodium dihydrogen phosphate was used to prepare the high phosphorus diet, sodium chloride was added to the control and low phosphorus diets to equalize the sodium intake. As a result, the concentration of chloride ions in the diets was in the following order: low phosphorus diet > control diet > high phosphorus diet (**Table 1**).

Recently, European Food Safety Authority (EFSA) has calculated the Dietary Reference Values (DRV) for chloride from the DRV for sodium, based on the assumption that chloride ions are consumed as sodium chloride [11]. This EFSA document does not specify the effects of excessive intake of chloride ions alone, independent of sodium or potassium. Since very little chloride are excreted in the feces [12] and are mostly absorbed in the gastrointestinal tract [11], it is possible that the blood concentration of chloride ions is maintained at a constant level by increasing urinary excretion rather than reducing absorption.

The water consumption and kidney weights of the rats fed the low phosphorus diet were significantly higher than those of the other two groups (**Table 2**). Although the exact amounts were not measured, it was observed that this group also produced more urine than the other two groups. On the other hand, there was no difference in the serum chloride ion concentrations among the three groups (**Table 3**) despite the large difference in chloride ion intake. These results suggest that rats in the low phosphorus group drank large amounts of water to excrete excess chloride ions in the urine, resulting in the accumulation of more water in the kidneys and an increase in their weight.

The main focus of the current experiment was to determine whether the changes in the kidney copper concentration that occurred in rats on the low-phosphorus diet were also observed on the high-phosphorus diet; in other words, whether increases or decreases in the phosphorus intake led directly to increases or decreases in the kidney copper concentrations. The results, as shown in **Table 4**, indicate that the renal copper concentrations do indeed increase or decrease in dependence on phosphorus intake. That is, the renal copper concentrations decreased when the phosphorus intake was low and increased when the phosphorus intake was high. To date, there have been no reported cases of such a phenomenon.

The body weights were lower in the low phosphorus diet group than in the other two groups. Feed efficiency was also decreased, suggesting that energy metabolism was not sufficiently maintained due to phosphorus deficiency at a dietary concentration of 0.15%. It has been reported that rats fed a low-phosphorus diet (0.2% phosphorus) show decreased serum phosphorus concentration, decreased bone mineralization rate, and growth inhibition [13]. The growth inhibition observed in rats fed a low-phosphorus diet (0.15%) in this study may be due to delayed bone formation resulting from decreased bone mineralization rate, in addition to decreased energy metabolism caused by phosphorus deficiency.

We have observed a decrease in the renal copper concentration in 8-week-old rats on a low-phosphorus diet or phosphate-binder without changes in the body weight or kidney weight [7-9]. Therefore, it is unlikely that the decrease in the renal copper concentration observed in rats on a low phosphorus diet is a secondary effect of growth inhibition.

On the other hand, in an experiment in which rats were given excess phosphorus, renal hypertrophy and calcification were observed when the dietary concentrations exceed about 1% [14]. Since no such abnormalities were observed at the 0.6% dietary phosphorus concentration in the present study, it can be concluded that no damage occurred as a result of excessive phosphorus intake. Thus, the increase or decrease in the renal copper concentration with changes in the phosphorus intake appears to be a primary effect of the increase or decrease in phosphorus intake.

Thus, in the present experiment, the increase in renal copper concentration associated with a high phosphorus diet was not particularly damaging to renal function. However, since copper accumulation in tissues can cause tissue damage via the Fenton reaction, the health effects of copper accumulation at higher doses of phosphorus than in the present study should be examined. In addition, the effects of decreased renal copper concentrations due to a low-phosphorus diet on the physiological functions of copper, such as the activity of copper-containing enzymes, should also be examined.

The liver copper levels were significantly lower only when fed a low phosphorus diet (**Table 4**). The serum copper concentrations also tended to decrease in the low phosphorus group, although not significantly (**Table 3**). Although these changes are minor compared to the renal concentrations, they may indicate a change in whole-body copper dynamics as phosphorus intake increases or decreases.

Phosphorus homeostasis involves intestinal absorption, bone absorption and formation, renal excretion, and renal tubular reabsorption. These are regulated by the parathyroid hormone and 1,25-dihydroxy vitamin D [15]. A marked decrease in the

urinary excretion of phosphorus was observed in rats with hypophosphatemia induced by the administration of phosphate-binders [7,8], suggesting that renal reabsorption of phosphorus may play an important role in phosphorus homeostasis. Phosphorus reabsorption in the renal tubules is regulated by fibroblast growth factor 23 (FGF23), and an increase in the serum phosphorus concentration increases the serum FGF23 concentration, while a decrease in the phosphorus concentration decreases the FGF23 concentration [16]. Such a change in the FGF23 concentration in response to an increase or decrease in the serum phosphorus concentration may have influenced the increase or decrease in the renal copper concentration. However, the relationship between FGF23 and urinary copper excretion is unknown. In addition, urine is not a major route of copper excretion, as copper is excreted *via* bile. Therefore, it is unlikely that FGF23 is involved in changes in the renal copper concentration.

Phosphate ions form insoluble salts with many metal ions. The significantly higher serum calcium concentration and the significantly higher liver iron and hemoglobin concentrations in the low phosphorus group (**Tables 3 and 4**) may indicate that the low phosphorus diet decreased the phosphate concentration in the gastrointestinal tract and increased the amounts of soluble calcium and iron that were absorbed.

Copper ions will also form insoluble salts with phosphate ions. If such insoluble salts are formed in the blood, they may not be filtered by the glomeruli of the kidney and may accumulate in the kidney. However, when the kidneys were divided into soluble and insoluble fractions and the copper concentrations were measured, they both changed in response to phosphorus intake (**Figure 1**). Furthermore, such insoluble salts could also be formed between iron or zinc ions and phosphate ions, but only copper showed significant changes in the kidney concentration. In other words, it is difficult to establish a mechanism by which insoluble salts of phosphate and copper were formed in the blood and accumulated in the kidneys.

As described above, changes in phosphorus intake may affect calcium and iron absorption. In particular, there have been several reports on the interaction between iron and copper and excess iron above the required level has been reported to inhibit copper absorption [17,18]. Accordingly, the present results may be mediated by changes in iron absorption rather than a direct effect of phosphorus. Therefore, it is necessary to reexamine copper concentrations in various organs when iron doses are varied, including changes in phosphorus in the body.

Acknowledgment

This study was supported by Grant-in-Aid for Scientific Research (22K055180).

References

[1] Takeda E, Yamamoto H, Yamanaka-Okumura H, Taketani Y: Dietary phosphorus in bone health and quality of life. Nutr Rev 70: 311-321, 2012.

[2] Chang AR, Anderson C: Dietary Phosphorus intake and the kidney. Annu Rev Nutr 37: 321-346, 2017.

[3] St-Jules DE, Goldfarb DS, Pompeii ML, Sevick MA: Phosphate additive avoidance in chronic kidney disease.Diabetes Spectr 30: 101-106, 2017.

[4] Tomson C: Vascular calcification in chronic renal failure. Nephron Clin Pract 93: c124-130, 2003.

[5] Ritz E: The clinical management of hyperphosphatemia. J Nephrol 18: 221-228, 2005.

[6] Yoshida M, Hosomi R, Kunimatsu M, Nakamura M, Fukunaga K, Kanda S, Nishiyama T: Phosphorus balance in rats with hypophosphatemia induced by lanthanum carbonate. Food Nutr Sci 3: 105-110, 2012.

[7] Yoshida M, Hosomi R, Noda H, Uemura K, Fukunaga K: Effect of lanthanum-induced low phosphorus status on tissue trace mineral contents. Proceedings of 15th International Conference on Heavy Metals in the Environment, Bargańska Ż, Beyer A, Klimaszewska K, Namieśnik J, Tobiszewski M, Rutkiewicz I (ed), Gdansk University of Technology, 2010, 870-872.

[8] Yoshida M, Yamakawa H, Yukawa N, Noguchi S, Fukunaga H, Nishiyama T: Transferrin saturation and tissue iron concentration in rats with high dose of ferric citrate. Biomed Res Trace Elem 24: 23-30, 2013.

[9] Noguchi S, Yukawa N, Fukunaga K, Nishiyama T, Yoshida M; Low phosphorus status contributes to high serum calcium and low renal copper levels in rats administered lanthanum. Trace Nutr Res 30: 31-34, 2013.

[10] Reeves PG, Nielsen FH, Fahey GC Jr: AIN-93 purified diets for laboratory rodents: final report of the American Institute of Nutrition ad hoc writing committee on the reformulation of the AIN-76A rodent diet. J Nutr 123: 1939-1951, 1993.

[11] European Food Safety Authority: Dietary reference values for chloride. EFSA J 17(9): 5779, 2019.

[12] Rose C, Parker A, Jefferson B and Cartmell E: The characterization of feces and urine: A review of the literature to inform advanced

treatment technology. Crit Rev Environ Sci Technol 45: 1827-1879, 2015.

[13] Baylink D, Wergedal J, Stauffer M: Formation, mineralization and resorption of bone in hypophosphatemic rats. J Clin Invest 50: 2519-2530, 1971.

[14] Hosomi R, Nakazawa C, Hagihara N, Fukunaga K, Yoshida M: Influence of the chemical form of phosphate salt and phosphorus level in the diet on kidney calcification and mineral balance in rats. J Jpn Health Med Assoc 29: 27-38, 2020.

[15] Bergwitz C, Jüppner H: Regulation of phosphate homeostasis by PTH, vitamin D, and FGF23. Annu Rev Med 61: 91-104, 2010.

[16] Gattineni J, Alphonse P, Zhang Q, Mathews N, Bates CM, Baum M: Regulation of renal phosphate transport by FGF23 is mediated by FGFR1 and FGFR4. Am J Physiol Renal Physiol 306: F351-358, 2014.

[17] Cohen NL, Keen CL, Lönnerdal B, Hurley L: Effects of varying dietary iron on the expression of copper deficiency in the growing rat: anemia, ferroxidase I and II, tissue trace elements, ascorbic acid, and xanthine dehydrogenase. J Nutr 115: 633-649, 1985.

[18] Ha JH, Doguer C, Wang X, Flores SR, Collins JF: High-iron consumption impairs growth and causes copper-deficiency anemia in weanling Sprague-Dawley rats. PLoS One 11(8): e0161033, 2016.

Metallomics Research 2022 (2) #MR202201

Note https://metallomicsresearch.brte.org

Elemental Imaging of the Rotula Bone of the Sea Urchin (*Strongylocentrotus intermedius*) using LA-ICP-MS and its Potential for Ecotoxicological Time-Scale Monitoring of Marine Environments

Takehisa Matsukawa[1,2*], Gaku Takebe[2], Ayano Kubota[1], Kazuyuki Saito[2], Atsuko Shinohara[1,3], Kazuhito Yokoyama[1,4]

[1]Department of Epidemiology and Environmental Health, Juntendo University Faculty of Medicine, Bunkyo-ku, Tokyo, Japan

[2]Department of Forensic Medicine, Juntendo University Faculty of Medicine, Bunkyo-ku, Tokyo, Japan

[3]Research Institute for Cultural Science, Seisen University, Shinagawa-ku, Tokyo, Japan

[4]Department of Epidemiology and Social Medicine, Graduate School of Public Health, International University of Health and Welfare, Minato-ku, Tokyo, Japan

Summary

Sea urchins do not actively travel long distances. Therefore, it is believed that their growth zones can be characterized to obtain information on marine environmental conditions. We analyzed trace elements in the rotula bones of Ezo-bahun-uni sea urchins (*Strongylocentrotus intermedius*) from brackish and salt water through two-dimensional elemental imaging using laser ablation inductively coupled plasma spectrometry (LA-ICP-MS). Before the LA-ICP-MS analysis, a conventional ICP-MS analysis was performed to determine the approximate elemental composition. The imaging results revealed different distribution patterns of Li, Sr, and Mn in the urchin rotula bones in brackish and salt water areas. Collectively, these findings support the use of sea urchins to monitor the inorganic composition of marine environments on an ecotoxicological time-scale.

Key words: Urchin, laser ablation inductively coupled plasma mass spectrometry, elemental imaging

Statements about COI: The authors declare no conflict of interest associated with this manuscript.

*Correspondence:
Takehisa Matsukawa
Department of Epidemiology and Environmental Health, Juntendo University Faculty of Medicine, 2-1-1 Hongo, Bunkyo-ku, Tokyo, 113-8421, Japan
Tel: +81 3 5802 1047
E-mail: tmatsuka@juntendo.ac.jp

Received: March 03, 2022
Accepted: August 03, 2022
Released online: August 18, 2022

Introduction

The elemental composition and concentration and isotopic composition in the hard tissues of marine organisms can be used to assess various factors of marine environments [1]. It is well known that the otoliths of fish grow throughout their life and retain elements incorporated in their annual growth bands. Analysis of specific parts of the otoliths can provide retrospective information on past environmental conditions [2, 3]. Fish otoliths are useful to assess the environment over a wide area of ocean as fish migrate.

On the contrary, benthic organisms, such as shellfish [4] and

coral [5] are considered to be beneficial for understanding the environmental conditions of specific marine areas. Sea urchins are also known as a good biological model for studying the marine environment, especially for pollution research [6-8]. Ternengo et al. suggested that benthic organisms can become a bioindicator of environmental trace elements because of their ecological relevance, benthic and relatively sedimentary lifestyle, rapid response, and high sensitivity to many types of contaminants [6]. For example, green sea urchins accumulate certain metals and can be used to monitor Ag, Cu, Fe, Hg, Pb, and Zn pollution in mining sites [7].

In this study, we focused on the rotula bone of the mouth organ (Aristotle's lantern) of sea urchin (*Strongylocentrotus intermedius*). This is because the bone continues to grow, similar to an otolith of fish, showing annual growth bands [9]; therefore, the content of elements in the bone reflects the environmental conditions when the bone developed. High-sensitivity elemental analysis by inductively coupled plasma mass spectrometry (ICP-MS) provides the contents of trace elements in biological samples, however, in-situ elemental analysis and reconstruction of mapping/imaging data is of great importance for precisely assessing the changes in elemental concentration over time, which can reflect the changes in marine environment. Hence, laser ablation ICP-MS (LA-ICP-MS) has been widely adopted to assess the bioaccumulation of metal elements in ecological and toxicological studies in humans, animals, and plants [10]. In the present study, we aimed to investigate the potential of the sea urchin as a bioindicator to chronologically monitor marine environments by comparing the elemental imaging data of its rotula bone from brackish and salt water using LA-ICP-MS.

Materials and Methods

Sample preparation for conventional ICP-MS

Ezo-bahun-uni sea urchins (*S. intermedius*) were purchased from two fishery cooperatives in Hokkaido, Japan. The first set of 10 sea urchin was collected from the brackish waters of Saroma, and the second set of 10 sea urchins was sourced from the salt waters of Yoichi. The 20 specimens in total (7-8 cm in length) were collected in June. Of the five rotula bones collected from each urchin (**Fig. 1a**), one was weighed and placed in a perfluoro-ethylene bottle containing 0.4 mL of 68% HNO_3 (ultrapure grade; Tama Chemicals Co., Kawasaki, Japan). The bones (n = 20) were immersed in HNO_3 overnight at 25 °C and then were added 0.2 mL of H_2O_2 (ultrapure grade; Tama Chemicals Co., Kawasaki, Japan). Microwave digestion was performed using Ethos Plus (Milestone General, Bergamo, Italy) under the following conditions; 250 W for 5 min, 0 W for 1 min, 250 W for 5 min, 400 W for 5 min, and 600W for 5 min. The volume of the digested sample was then adjusted to 1.0 mL with ultrapure water. The fixed-volume solution was diluted 25 times in 1.5% nitric acid and 20 ng/mL Sb was added as an internal standard. The containers for samples and all measured solutions were rinsed with ultrapure water (18.2 MΩ/cm) after pre-cleaning with nitric acid.

Conventional ICP-MS analysis

The elemental concentrations in each diluted solution were determined using an inductively coupled plasma mass spectrometer

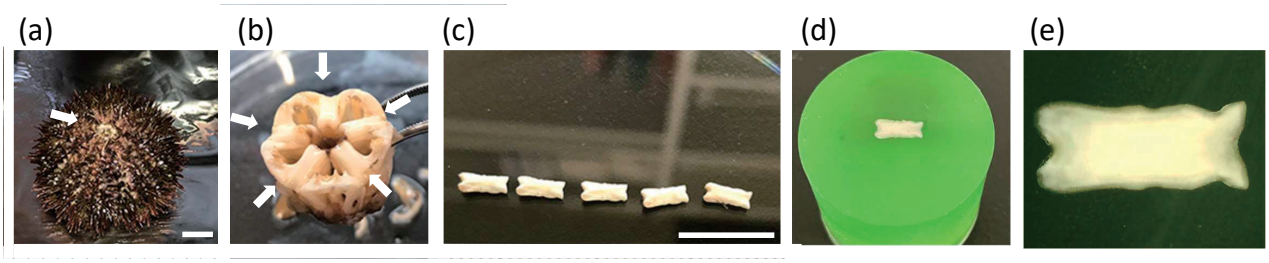

Fig. 1. **Pretreatment of rotula bones for LA-IC-MS analysis**
(a) the mouth organ "Aristotle's lantern" was harvested from each sea urchin (white arrow, scale bar = 1 cm) ;
(b) five rotula bones (white arrows) were collected from the upper side of the mouth organ of each sea urchin ;
(c) the five rotula bones were dried, and one was selected (n = 10) and digested for conventional ICP-MS analysis (scale bar = 1 cm) ;
(d) a second rotula bone (n = 3) was embedded in a resin mold and polished using diamond slurry ;
(e) by placing the polished surface facing the laser source in the LA sample chamber, LA-ICP-MS analysis was performed.

(ICP-MS; Agilent 8800; Agilent Technologies, Tokyo, Japan). ICP-MS were calculated using 0, 0.4, 4.0, and 40.0 ng/mL of the multi-element standard solutions XSTC-1 and XSTC-13 (SPEX Industries Inc., NJ, USA) diluted with 0.5% nitric acid. The concentration of 45 elements (Ag, Al, As, Ba, Bi, Ca, Cd, Ce, Co, Cr, Cs, Cu, Dy, Er, Eu, Fe, Ga, Gd, Ho, In, K, La, Li, Lu, Mg, Mn, Na, Nd, Ni, Pb, Pr, Rb, Sc, Se, Sm, Sr, Tb, Th, Tl, Tm, U, V, Y, Yb, and Zn) was measured using a standard calibration method with the signal intensity of Sb as the internal standard. The elemental concentrations in each tested rotula bone were determined using the obtained mean elemental contents and the dry weight of the digested bone.

Statistical analysis

The element concentrations in rotula bone of urchins from brackish (n = 10) and salt (n = 10) waters, determined using conventional ICP-MS analysis, were compared using the unpaired Student t-test in Microsoft Excel for Microsoft 365 MSO (16.0.14228.20216). The level of significance was set at $p < 0.05$.

Sample prepatation for LA-ICP-MS

The rotula bones (**Fig. 1b-d**) of three urchins from each sampling area were imaged using LA-ICP-MS. One bone per urchin was embedded in epoxy resin (Technovit 4071; Kulzer, Wehrheim, Germany), and the epiphyseal side of the bone was polished using diamond pads (Cameo® Disk Platinum Type 1 and Type 3; Leco Corporation, St Joseph, MI, USA). Next, the bones were ultrasonically cleaned and polished on a polishing cloth using diamond slurry (6 μm and 9 μm in diameter) (Maruto Co., Tokyo, Japan). Following a second wash with ultrapure water, the bones were observed under a stereomicroscope to estimate the age of the urchin from the ring pattern on the polished surface as described by Watanabe and Takada [11].

LA-ICP-MS analysis

Elemental imaging was performed via multiple-line profiling LA-ICP-MS analysis with the parameters listed in **Table 1**. The signal intensity (count per second) obtained by ICP-MS was reconstructed using iQuant2 (Ver.2018 Apr) [12] to generate elemental images. The range of the color bar was adjusted for each element to get better visualization.

Table 1. | Instrumentation and operational settings

Laser (New Wave Research NWR213)		ICP-MS (Agilent 8800)	
Wavelength	213 nm	RF incident power	1600 W
Pulse energy	10%	Plasma gas flow rate	15.0 L min^{-1}
Fluence	4.0 J cm^{-2}	He carrier gas flow rate	0.80 L min^{-1}
Repetition rate	10 Hz	Ar carrier gas flow rate	0.95 L min^{-1}
Spot size	50 × 50 μm (square)	Monitored isotopes	^{7}Li, ^{31}P, ^{43}Ca, ^{52}Cr, ^{55}Mn, ^{66}Zn, ^{88}Sr,
Scan speed	35 μm s^{-1}		^{139}La, ^{140}Ce, ^{141}Pr, ^{146}Nd, ^{147}Sm
Stabilizer	not used	Data acquisition mode	Time-resolved analysis
		Dwell time	^{7}Li, ^{52}Cr ^{88}Sr, ^{139}La, ^{140}Ce, ^{141}Pr, ^{146}Nd, ^{147}Sm : 0.05 sec
			^{66}Zn: 0.05 sec
			^{55}Mn: 0.01 sec
			^{31}P, ^{43}Ca: 0.0005 sec

Results and Discussion

Data obtained from conventional ICP-MS analysis (mean ± S.D. [μg/g]) showed that Mn (Saroma: 4.15 ± 2.62, Yoichi: 0.77 ± 0.60) and La (Saroma: 0.01 ± 0.005, Yoichi: 0.005 ± 0.002) concentrations were significantly higher in the Saroma brackish water group than in the Yoichi salt water group ($p < 0.05$). Conversely, Li (Saroma: 1.49 ± 0.39, Yoichi: 2.16 ± 0.64) and Sr (Saroma: 796.1 ± 186.9, Yoichi: 1047.0 ± 275.0) concentrations were significantly higher in the salt water group than in the brackish water group ($p < 0.05$). The strata around Saroma are known to be rich in Mn [13], and it is possible that Mn was brought in from river water. For Li and Sr, it was assumed that their concentrations were lower in Saloma because they were diluted in fresh water compared to seawater. The other trace elements measured did not show sufficient concentrations for comparison. Subsequently, we performed LA-ICP-MS analysis of aforesaid four elements that exhibited the differences between the two areas in ICP-MS analysis mainly, in addition to Ca as a major component of bone tissue.

Sea urchin age was estimated by measuring the number of growth band on the sampled bones (**Fig. 2**). Approximately 5 bands were clearly observed were observed only in the brackish water group, indicating that the Saroma sea urchins were 5-6 years old. On the contrary, clear growth bands were not observed in salt water sea urchin samples. Narvaez et al. [14] reported that the absence of distinct growth bands in sea urchins was dependent on their growth environment (e.g., food availability); the sea urchin selected for the present study may have been similarly affected by food availability in their habitat.

The LA-ICP-MS analysis (**Fig. 3**) showed that Ca, a major component of bone, was homogeneously distributed throughout the bone, whereas Li, Sr, and Mn were distributed in a ring along the growth bands. The integrated signal intensity from LA-ICP-MS did not always match the concentration results from the conventional ICP-MS, which may be due to heterogeneous distribution in the bone. Although the mechanisms underlying the uptake of these elements and their ring-shaped accumulation in the rotula bones of sea urchin remain unknown, these phenomena exhibit a certain periodicity. The cyclic repeated pattern of these elements in sea urchin bones may be influenced by the seasonal changes of the salt water environment, as observed in fish [2,3].

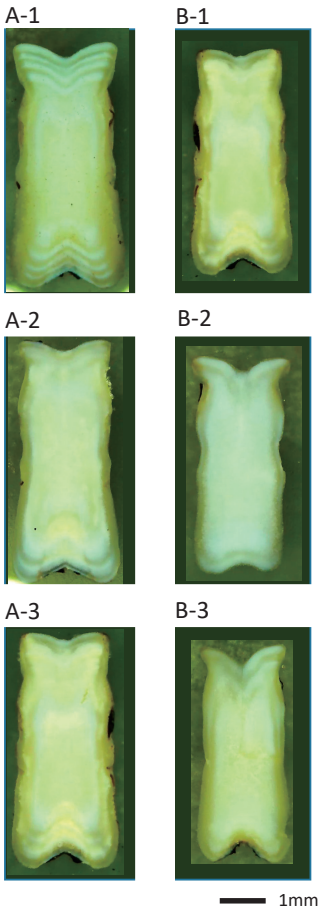

Fig. 2. **Observation image by optical microscope rotula bone of *Strongylocentrotus intermedius***
A-1, -2, and -3 are samples from Saroma (brackish water); B-1, -2, and -3 are samples from Yoichi (salt water). Scale bar = 1mm.

Elemental imaging of sea urchin rotula bones offers the possibility to monitor the marine environment chronologically on an ecotoxicological time scale. The longevity of *S. intermedius* is estimated to be 6-10 years [15]. Our findings indicate that this method is particularly effective on specimens from brackish waters where there are seasonal variations in elemental composition exists. The analysis of sea urchins by LA-ICP-MS is also useful to assess contamination by toxic metals and radioisotopes, and to assess the bioavailability of inorganic nutrients in the marine environments over time.

Conclusion

We used LA-ICP-MS to determine the distribution of elements in the rotula bones of *S. intermedius* collected from brackish water and seawater. Elemental imaging of sea urchin rotula bones suggested that they could be used to monitor the marine environment over time. In this study, the number and size of the sea urchin used were limited, and future analyses of more sea urchin in the same region using this methodology may provide additional information on the ecotoxicological time-scale changes in the marine environment.

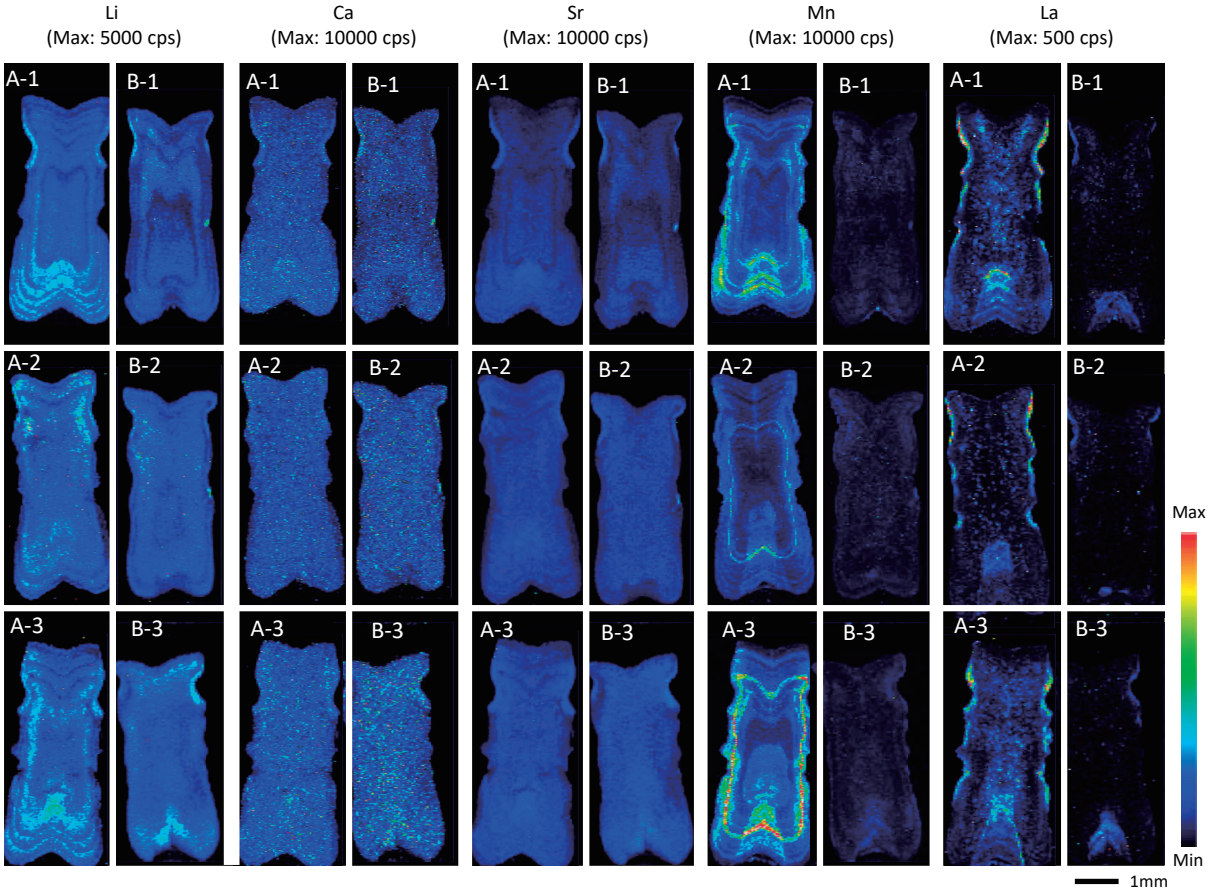

Fig. 3. **Distribution of inorganic elements in the rotula bones of *Strongylocentrotus intermedius***
each sea urchin sample was analyzed simultaneously using LA-ICP-MS. A-1, -2, and -3 are samples from Saroma (brackish water); B-1, -2, and -3 are samples from Yoichi (salt water). cps, count per second.

Acknowledgments

We are grateful to Ms. Shizuka Iwasaki for technical assistance. This work was partly supported by JSPS KAKENHI Grant Number IH19H01081.

References

[1] McMahon KW, Hamady LL, Thorrold SR: A review of ecogeochemistry approaches to estimating movements of marine animals. Limnol Oceanogr 58: 697-714, 2013.

[2] Arai T, Hirata T: Differences in the trace element deposition in otoliths between marine- and freshwater-resident Japanese eels, *Anguilla japonica*, as determined by laser ablation ICPMS. Environ Biol Fishes 75: 173-182, 2006.

[3] Palace VP, Halden NM, Yang P, Evans RE, Sterling G: Determining residence patterns of rainbow trout using laser ablation inductively coupled plasma mass spectrometry (LA-ICP-MS) analysis of selenium in otoliths. Environ Sci Technol 41: 3679-3683, 2007.

[4] Raith A, Perkins W, Pearce N, Jeffries T: Environmental monitoring on shellfish using UV laser ablation ICP-MS. Fresen J Anal Chem 355: 789-92, 1996.

[5] Amir L, Mohamed C: A short review of coral resilience in a changing marine environment. Poll Res 36: 693-708, 2017.

[6] Ternengo S, Marengo M, El Idrissi O, Yepka J, Pasqualini V, Gobert S: Spatial variations in trace element concentrations of the sea urchin, Paracentrotus lividus, a first reference study in the Mediterranean Sea. Mar Pollut Bull 129: 293-298, 2018.

[7] Søndergaard J, Hansson SV, Mosbech A, Bach L: Green sea urchins (*Strongylocentrotus droebachiensis*) as potential biomonitors of metal pollution near a former lead-zinc mine in West Greenland. Environ Monit Assess 191: 538, 2019.

[8] LaVigne M, Hill T, Sanford E, Gaylord B, Russell A, Lenz E, Hosfelt J, Young M: The elemental composition of purple sea urchin

(*Strongylocentrotus purpuratus*) calcite and potential effects of pCO_2 during early life stages. Biogeosci 10: 3465-77, 2013.

[9] Balboa C, Molinet C, Barahona N, Díaz PA, Subiabre D, Gebauer P: Using growth ring formation to study growth patterns of exploited sea urchin (*Loxechinus albus*) populations. Fish Res 201: 88-97, 2018.

[10] Hereu B: Movement patterns of the sea urchin Paracentrotus lividus in a marine reserve and an unprotected area in the NW Mediterranean. Marine Ecol 26: 54-62, 2005.

[11] Watanabe S, Takada: Age determination by rotula of the purple sea urchin Anthocidaris crassispina. Bulletin of Nagasaki Prefectural Institute of Fisheries 41: 21-25, 2015.

[12] Suzuki T, Sakata S, Makino Y, Obayashi H, Ohara S, Hattori K, Hirata T: iQuant2: Software for rapid and quantitative imaging using laser ablation-ICP mass spectrometry. Mass Spectrom 7: A0065, 2018.

[13] Choi JH, and Hariya Y: Geochemistry of manganese deposits in the Tokoro Belt, northeastern Hokkaido. Mining Geol 40: 159-173, 1990.

[14] Narvaez CA, Johnson LE, Sainte-Marie B: Growth bands are an unreliable indicator of sea urchin age: Evidence from the laboratory and the literature. Limnol Oceanogr Meth 14: 527-541, 2016.

[15] Agatsuma Y: Ecology of *Strongylocentrotus intermedius*. Dev Aquac Fish Sci 37: 427-441, 2007.